Electrospray Thruster Plume Characterization via Physics-Informed Machine Learning

McKenna J. D. Breddan*
University of California, Los Angeles, Los Angeles, CA, 90095, USA

Richard E. Wirz^{†‡}
University of California, Los Angeles, Los Angeles, CA, 90095, USA
Oregon State University, Corvallis, OR, 97331, USA

To extend electrospray thruster lifetime and improve performance, we must understand the relationship between particle emission conditions and the resulting evolved plume. To this end, we apply machine learning algorithms to simulated electrospray particle data to investigate correlations between particle properties at emission and further downstream. The strength of predictive ability and correlation rankings with emission properties are presented for final plume angle, among other final properties, and discussed in relation to the physical forces governing electrospray plume evolution. Illuminated correlations between particle properties inform diagnostic design by determining which properties offer the most insight towards predicting other properties.

Nomenclature

Subscripts

- A Applied electric field
- C Coulomb
- f Final
- I Inertial
- i Initial/Emission
- *Im* Image charge
- r Radial
- x Lateral, x component
- y Lateral, y component
- z Axial

Symbols

- ϵ_0 Permittivity of vacuum [F/m]
- \hat{p} Predicted value
- λ Breakup wavelength [m]
- ϕ Potential [V]
- ρ Density [kg/ m^3]
- r Separation radius [m]
- v Velocity [m/s]
- x Position [m]
- θ Plume angle [deg]

ANRMSE Absolute normalized root mean squared error

- C_D Coefficient of drag
- d Diameter [m]
- E Electric field [V/m]
- F Force [N]
- l Distance from jet tip to reference point for emission velocity angle [m]

^{*}Ph.D. Candidate, Mechanical and Aerospace Engineering, mjdavis325@g.ucla.edu, AIAA Student Member

[†]Adjunct Professor, Mechanical and Aerospace Engineering, wirz@ucla.edu, AIAA Associate Fellow

[‡]Boeing Professor, Aerospace Engineering, richard.wirz@oregonstate.edu, AIAA Associate Fellow

m Mass [kg]

Number of samples

n Number of droplets in plume

p True value

q Charge [C]

R Coefficient of determination

t Time [s]

x Position coordinate, x component [m]

y Position coordinate, y component [m]

z Position coordinate, z component [m]

I. Introduction

Electrosprays enable a diverse range of technologies, from mass spectrometry [1] to targeted drug delivery [2], electrostatic purification [3–5], 3D printing [6, 7], and spacecraft propulsion [8, 9]. A wealth of electrospray data has been generated through experimental observations and computational simulations such that machine learning (ML) algorithms can now be employed to assist in electrospray research. The literature presents such ML applications to experimental data, including the prediction of mean particle size[10] and estimations of ionization efficiency[11]. This publication summarizes the first application of ML algorithms to simulated electrospray particle data. Three primary benefits of utilizing machine learning with simulated electrospray particle data are identified:

- 1) ML regression models can form meta-models for the larger particle tracking models used to generate the training data, thereby saving computational expense of additional runs of the larger model.
- 2) ML regression algorithms can predict unknown final (at the collector plate) particle properties given emission properties, or emission properties and known final properties.
- 3) Random Forest models yield feature rankings which identify correlations between particle properties.

We additionally discuss the role of machine learning in optimizing electrospray diagnostic design by determining which particle properties provide the most insight towards other properties. Finally, we invite the application of the presented machine learning analysis to further simulated electrospray tracking data in the literature [12–16].

II. Methods

The particle data used in this study were obtained from University of California, Los Angeles (UCLA) Plasma, Energy & Space Propulsion Laboratory (PESPL) Discrete Electrospray Lagrangian Interaction (DELI) Model plume evolution simulations using experimental conditions from Gañan-Calvo et al. [12], for which case the DELI Model was validated in a previous publication [17]. Each data sample includes particle mass m, charge q, 3D emission coordinates (x_i, y_i, z_i) , 3D emission velocity $(v_{xi}, v_{y_i}, v_{z_i})$, final positional plume angle θ_f , 3D final velocity $(v_{xf}, v_{y_f}, v_{z_f})$, and final potential ϕ_f . All properties are direct outputs of DELI simulations with the exceptions of plume angle:

$$\theta_f = \arctan\left(\frac{\sqrt{x_f^2 + y_f^2}}{z_f}\right),\tag{1}$$

and final potential:

$$\phi_f = \frac{\frac{1}{2}m|\mathbf{v_f}|^2}{q},\tag{2}$$

where 3D final coordinates (x_f, y_f, z_f) are direct simulation outputs. Simulated axial emission coordinate z_i was constant such that it is not included in the feature set for machine learning studies. DELI Model simulations did not include particle breakup[18–21] such that particle mass and charge are unchanged from emission at the downstream collector plate. Particles were advanced with the equation of motion:

$$m\frac{d^{2}\mathbf{x}}{dt^{2}} = q(E_{A} + E_{C} - E_{I}) - F_{D} = qE_{A} + \frac{q}{4\pi\epsilon_{0}} \sum_{i=1}^{n} \frac{q_{i}r_{i}}{|\mathbf{r_{i}}|^{3}} - \frac{q^{2}}{4\pi\epsilon_{0}} \frac{r_{I}}{|\mathbf{r_{I}}|^{3}} - C_{D} \frac{\pi}{8} \rho d^{2}\mathbf{v}|\mathbf{v}|,$$
(3)

where E_A is the applied electric field, E_C is the Coulomb electric field generated by the charged plume particles, E_I is the electric field created by image charges induced in the collector plate, F_D is the drag force, ϵ_0 is the permittivity of

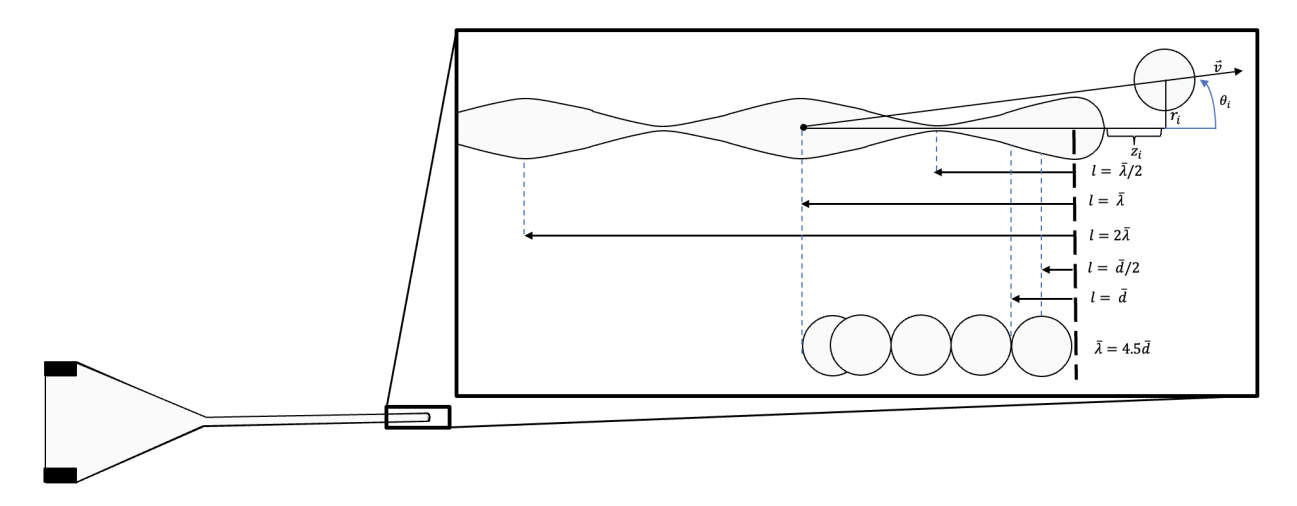


Fig. 1 Emission velocity vector direction is the angle between particle emission position and a reference point in the jet distance l upstream from the jet tip, where l varies from one mean particle radius to one mean breakup wavelength. An example emission velocity vector is shown for $l = \overline{\lambda}[26]$.

vacuum, n is the total number of particles in the plume, $\mathbf{r_i}$ is the separation vector between particles ($\mathbf{r_I}$ is the separation vector between a particle and its image charge in the collector plate), C_D is the coefficient of drag, ρ is the density of the surrounding fluid, d is particle diameter, and \mathbf{v} is particle velocity.

Particle emission has been experimentally observed to occur at an angle tilted from the vertical axis[22–24], such that particles have radial components to their velocity vectors. This observed tilt is contrasts with the theoretical ideal electrospray behavior in which droplets are emitted with strictly axial velocity. Initial machine learning investigations displayed a correlation between the range of simulated particle emission velocity angles and the accuracy of machine learning regressions on particle data. To further investigate the influence of velocity emission angle on electrospray particle data machine learning regressions, we analyzed multiple cases of particle data which fall into two categories:

- 1) Strictly axial emission velocity, and
- 2) Non-zero radial emission velocity.

For the cases with a radial component to emission velocity, Figure 1 displays the means of determining emission velocity angle, set equal to emission positional angle:

$$\tan\left(\frac{v_{ri}}{v_{zi}}\right) = \tan\left(\frac{r_i}{l}\right),\tag{4}$$

where r_i is the emission radial coordinate, v_{ri} is the emission radial velocity component, and l is the distance between the jet tip from which particles are emitted and the upstream reference point for calculating velocity emission angle. This distance was varied from one mean particle radius $l = \overline{d}/2$ to two mean jet breakup wavelengths $l = 2\overline{\lambda}$, where mean breakup wavelength $\overline{\lambda} = 4.5\overline{d}$ [12, 25]. Data sets for each velocity angle emission simulation case included 35,000 unique particle trajectory data samples.

Six different ML models were applied to the Lagrangian electrospray particle data: Python package scikit-learn library (v1.1.2)[27] Random Forest (RF), Support Vector Regression (SVR), k-Nearest Neighbor(kNN), and Multilayer Perceptron (MLP) models; the py-xgboost library (v1.6.2)[28] Extreme Gradient Boosting (XGBoost) model; and the lightgbm library (v3.3.2)[29] Light Gradient Boosting Machine (LGBM) model. Particle trajectory data were first filtered for uniqueness, then randomly shuffled in order using the scikit-learn shuffle function, and finally scaled using the scikit-learn StandardScaler function to fit a standard scaler to the training feature data and apply it to the testing feature data. The scikit-learn train_test_split function was used to reserve 80% of the particle dynamics data for training the machine learning models, and the remaining 20% for testing.

Model performance was analyzed using the coefficient of determination (R^2) and the absolute-normalized root mean squared error (ANRMSE):

$$R^{2} = \sqrt{\frac{\sum_{i=1}^{N} (\bar{p}_{i} - \hat{p}_{i})^{2}}{\sum_{i=1}^{N} (\bar{p}_{i} - p_{i})^{2}}},$$
(5)

$$ANRMSE = \frac{\sqrt{\frac{\sum_{i=1}^{N} (p_i - \hat{p}_i)^2}{N}}}{\frac{N}{|p_i|}},$$
 (6)

where N is the number of samples, p_i is the true value of the variable being predicted, \hat{p}_i is the value predicted by an ML model, and $\overline{p_i}$ is the mean of the true values. Hyperparameter tuning was conducted on all machine learning models to optimize coefficients of determination through 5-fold cross validation.

III. Results and Discussion

Our machine learning analysis was informed by an understanding of the physical forces governing electrospray evolution. The applied electrostatic force dominates axial droplet motion[30], whereas Coulomb interactions between particles are the primary radial expansion force on plume particles[30, 31], especially in the region near emission[32]. The positional displacement resulting from applied electrostatic acceleration has a linear relationship with particle mass and charge:

$$\Delta \vec{x_E} = \frac{q}{m} \int \int E_A dt^2, \tag{7}$$

whereas Coulomb displacement,

$$\Delta \overrightarrow{\mathbf{x}_C} = \frac{q}{m4\pi\epsilon_0} \int \int \sum_{i=1}^n \frac{q_i r_i}{|\mathbf{r}_i|^3} dt^2, \tag{8}$$

is nonlinear and heavily dependent on stochastic interactions with near-neighbor (low separation radius $|r_i|$) particles. Inertia also contributes linearly to particle displacement:

$$\Delta \vec{x_I} = \vec{v_i} t, \tag{9}$$

where $\overrightarrow{v_i}$ is emission velocity. Therefore, when particles are emitted with non-zero radial velocity, inertia contributes a linear component to particle radial motion which is otherwise dominated by nonlinear Coulomb interactions. Wider emission velocity angles ranges, which correspond to smaller distances l between the jet tip and the upstream reference point for velocity emission angle in Fig. 1, contribute stronger radial inertia to droplet trajectories and thereby linearize radial particle dynamics. A comparison of the pathlines of 30 particles from the strictly axial and the widest angle range emission velocity cases is presented in Fig. 2. The linearization of particle radial displacement due to inertia is clearly visible in the non-zero radial emission velocity case (red pathlines). Likewise, the process of Coulomb interaction driven particle radial displacement is visible in the strictly axial emission case (blue pathlines): particles are displaced from the axis of emission at varying distances downstream of emission in a non-linear manner following stochastic interactions with neighboring particles.

We utilized the correlative and predictive power of the six machine learning algorithms presented in Sec. II to predict final particle properties $(\theta_f, v_{xf}, v_{yf}, v_{zf}, \phi_f)$ from emission particle properties (m, q, x_i, y_i) . The literature lacks a known closed-form equation relating particle properties at emission and downstream of emission, yet includes a surplus of simulated electrospray particle trajectory data, creating an ideal environment for the application of machine learning regression algorithms to this data. Fig. 3 presents R^2 scores for the prediction of each final particle property using emission particle properties as input features for the strictly axial and widest angle range emission velocity cases. The performance metric results are presented with bar color corresponding to predictive model, such that the range of performance can be seen among the six ML models.

In the solely axial emission velocity case, no algorithms predict final particle properties reliably with all coefficients of determination below 0.7. In contrast, there is significant correlation between emission and final particle properties in the non-zero radial velocity emission case. All models predict the final lateral velocity components with $R^2 \ge 0.79$ (and $ANRMSE \le 0.3$) and final angle with $R^2 \ge 0.77$ (and $ANRMSE \le 0.25$). Coefficients of determination exceeding 0.75 are comparable with the higher R^2 scores from other machine learning studies of electrosprays [10, 11]. The ML models thereby have potential to serve as meta-models for the larger Lagrangian model in yielding final angle and final lateral velocity components given particle emission properties for the widest angle range velocity emission case. Our conclusions on displacement linearity from the governing force analysis support these differences between machine learning predictive capabilities between the velocity emission angles cases. In the non-zero radial emission velocity case, particle dynamics have a significant linear component from inertia which allows ML models to better correlate final particle properties with emission properties. In the strictly axial emission velocity case, the dominance of nonlinear

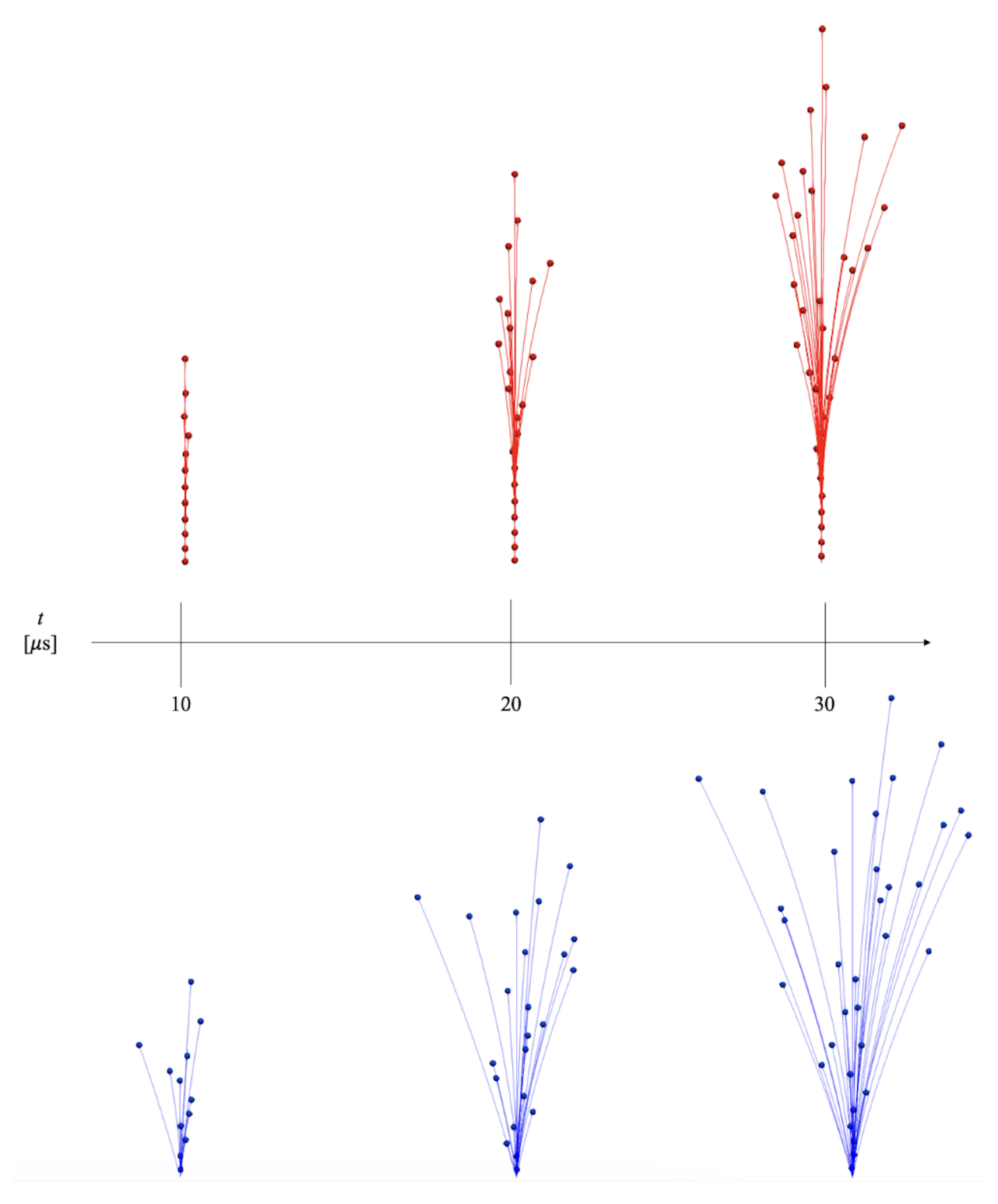
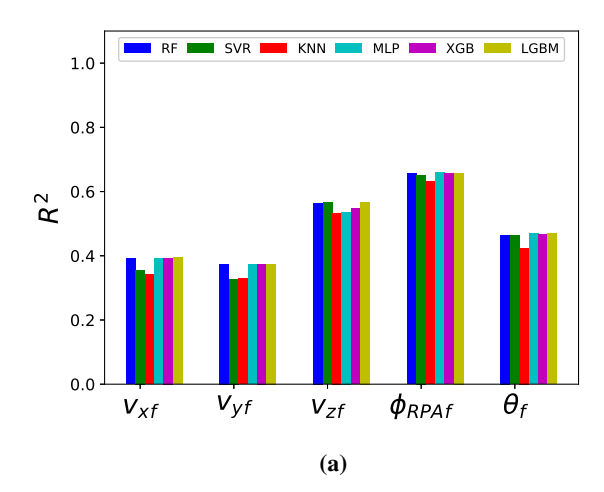


Fig. 2 Pathlines are shown for every other of 60 emitted particles over a 30 µ sec period for the solely axial emission velocity (red) and the widest angle emission velocity (blue) cases[26].

 $Coulomb \ forces \ on \ particle \ trajectories \ preclude \ ML \ models \ from \ predicting \ final \ particle \ properties \ exclusively \ from \ emission \ properties.$

Final particle angle is a key property of interest for electrospray thruster lifetime due to propellant overspray failure



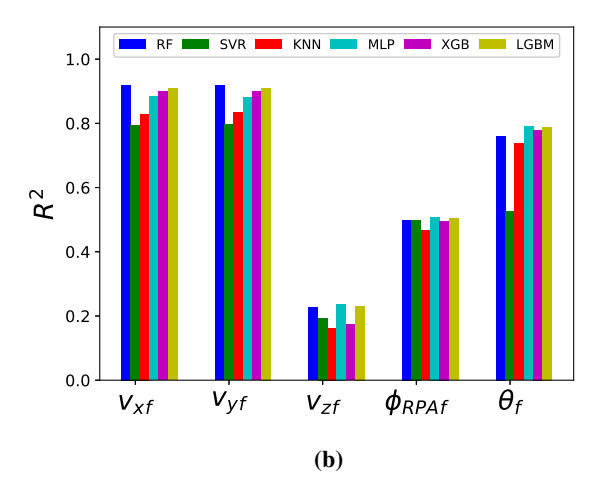
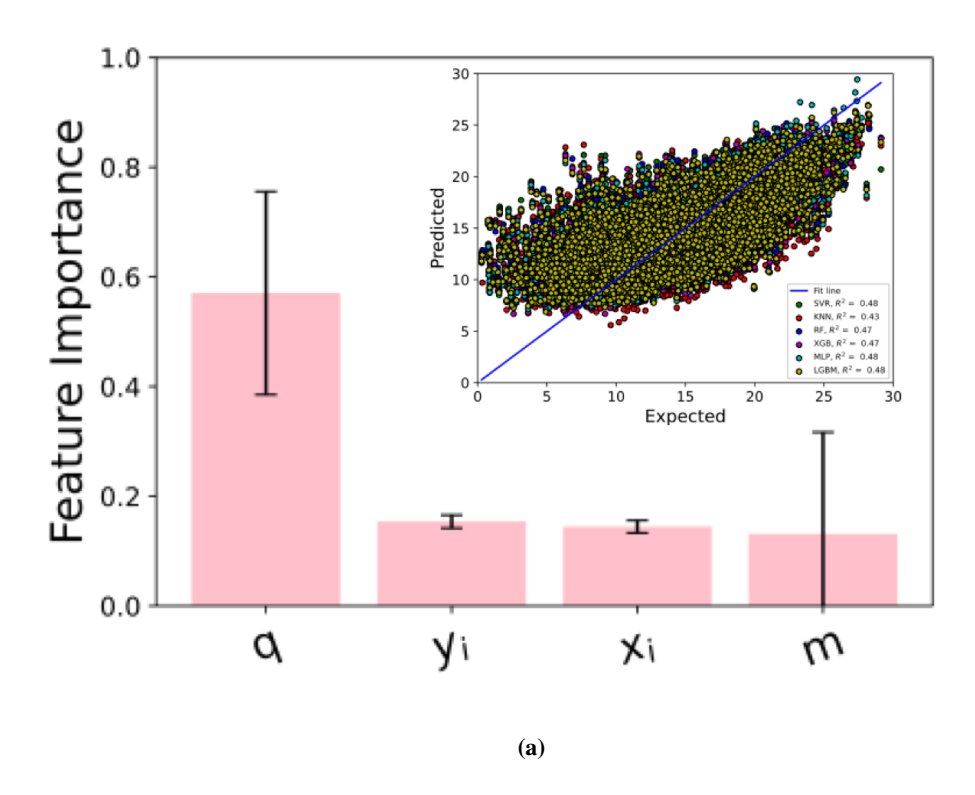


Fig. 3 Coefficients of determination for the prediction of each final particle property given all emission particle properties for the (a) strictly axial emission velocity case and the (b) widest angle emission velocity case with color corresponding to ML algorithm[26].

mechanisms[33, 34]. Therefore, we further analyzed correlations between emission particle properties and final angle identified by Random Forest (RF) algorithm feature rankings for both emission velocity cases, presented in Fig. 4. The fits of prediction of final angle for all six machine learning models are showcased in the inset plot of Fig. 4. The feature rankings for the solely axial emission velocity case exclude velocity components v_{xi} , v_{yi} , and v_{zi} because they are constants. Although final angle cannot be reliably predicted from emission properties for the solely axial emission velocity case due to the non-linear nature of particle trajectories, RF feature rankings enforce the narrative of plume expansion dominated by charge-dependent Coulomb collisions [12, 15, 17, 35] by revealing charge to be the dominant feature for predicting final angle. In the non-zero radial emission velocity case, RF feature rankings support the dominance of inertia by revealing emission lateral velocity components to be the dominant features for predicting final positional angle.

Feature rankings for additional final particle properties also support established understandings of the physics of plume evolution. Figures 5a and 5b display the feature rankings for final axial velocity and final potential, respectively, given emission properties as input features. Particle charge has dominant feature importance for the prediction of final axial velocity, stemming from the direct relationship between particle charge and the applied electrostatic force dominating particle axial motion. Particle charge is also the dominant feature for predicting final potential, and mass has secondary feature dominance, both of which are expected given the linear relationship between these properties and potential given in Eq. 2.

For the nonlinear particle dynamics case following solely axial emission velocity, all six presented machine learning models failed to predict final particle properties with statistically significant accuracy given only emission particle properties as input features. However, when final particle angle θ_f is added to the input feature list alongside emission particle properties, stronger performance is achieved in predicting other final particle properties. Final axial velocity and final potential were most reliably predicted from the final property set given only emission properties as shown in Fig. 3a. When also given final angle, these variables can be predicted with high coefficients of determination: $R^2 > 0.88$ for final axial velocity and $R^2 > 0.93$ for final potential for all models. Therefore, these ML models can create a limited meta-model for the full Lagrangian model to obtain final axial velocity and final potential given emission properties and final angle. The improvement in predictive ability from adding final angle to the input feature set highlights a strong correlation between final angle and other final particle dynamic properties. This trend has been observed experimentally, with plume profile measurements demonstrating angular dependence [34]. Figures 5c and 5d give feature rankings for final axial velocity and final potential, respectively, given emission properties and final angle as input features. Final angle is significantly dominant over all other features for the prediction of final axial velocity, displaying a strong correlation between final angle and final axial velocity. While charge remains dominant in the final potential feature ranking, final angle has feature importance nearly equal to that of mass, to which potential has an indirect relationship following Eq. 2.



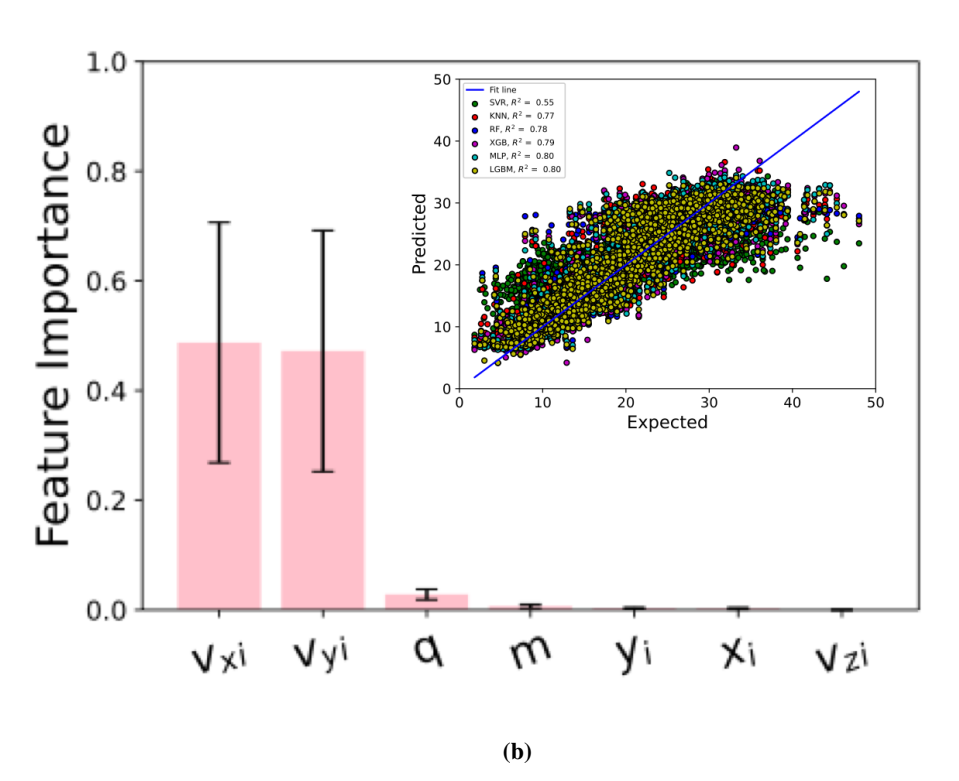


Fig. 4 Random Forest feature rankings for final angle regression for the (a) strictly axial emission velocity case and the (b) widest angle emission velocity case with error bars showing the range among individual decision trees in the forest. Inset plots showcase the fit for predicting final angle from all six ML models. Figure adapted from [26].

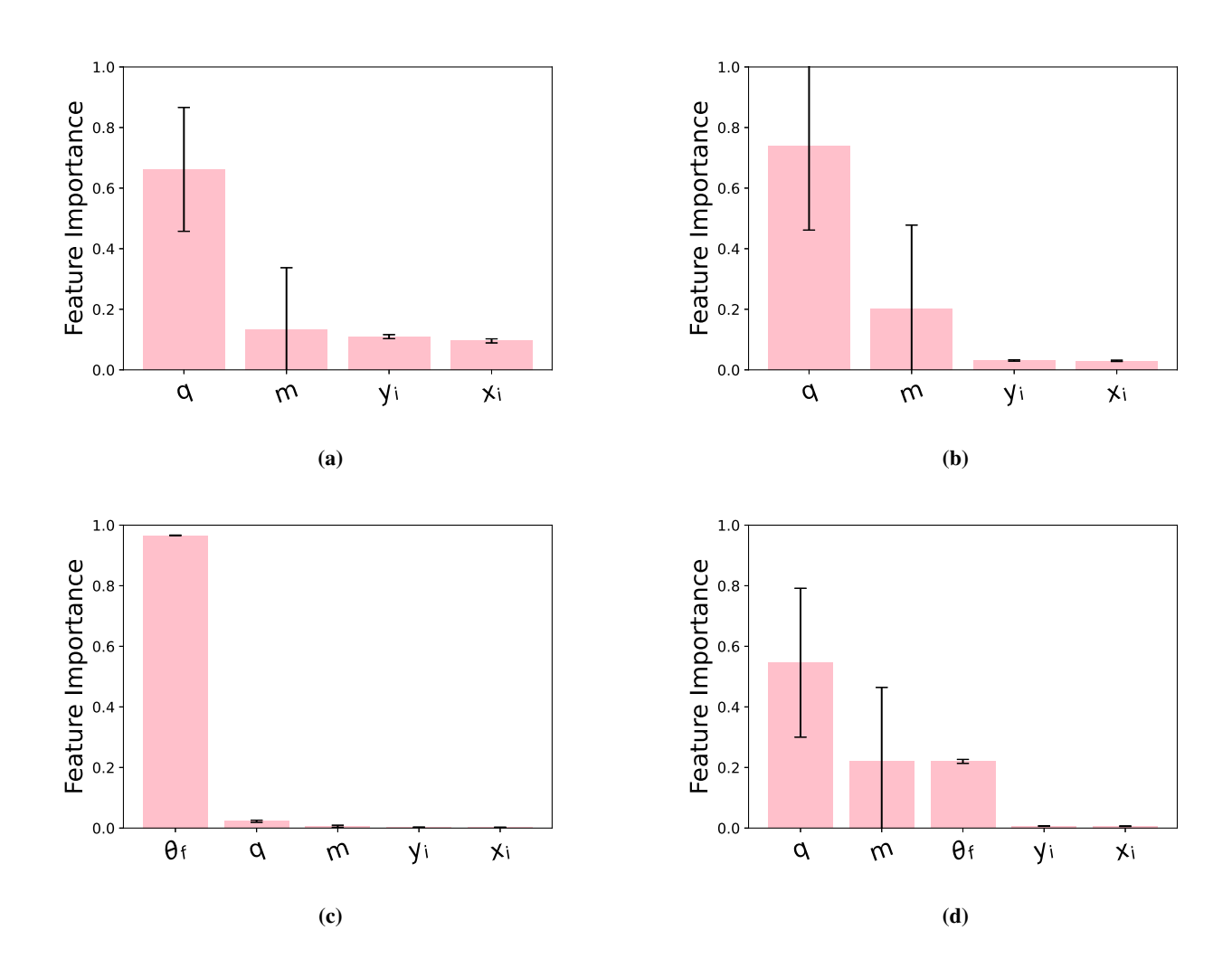


Fig. 5 Random Forest feature rankings for final axial velocity (a,c) and potential (b,d) given only emission properties (a,b) and also given final angle (c,d) with error bars showing range among individual decision trees in the forest[26].

The correlations between particle properties identified by ML models have diagnostic design value because they inform researchers of which particle properties yield the most insight towards other particle properties. In the presented strictly axial emission velocity case, final angle was found to be strongly correlated with both final axial velocity and final potential, such that for this case, an angular profile measurement from a simple Faraday probe[36, 37] could be used with the machine learning meta-model to yield final axial velocity and final potential measurements typically obtained by Time Of Flight and Retarding Potential Analyzer devices.

IV. Conclusion

We have demonstrated the utility of applying machine learning algorithms to simulated electrospray particle data obtained by the UCLA DELI Model in a physics-informed framework. The methods we present are widely applicable to data from other electrospray plume simulations[12–16].

We propose that the prediction accuracy of our methods can be further improved by:

- 1) increased volume of training data,
- 2) increased variance among particle emission property feature data sets so that emitted particles are more distinguishable from one another, such as increased mass polydispersity or charge inhomogeneity,
- 3) expanding the feature set to include additional particle emission properties,
- 4) the improvement of Lagrangian particle tracking models to more closely match the physical reality of electrospray plume evolution, such as including particle coalescence and breakup [38, 39] and secondary electron emission [40, 41].

To the first point, we note that there is a sparsity of simulated particle data with high final angle, which is also observed experimentally, due to the relative lack of particle flux at high positional angles[34, 36]. This angular data bias leads to higher prediction error by ML models for high-angle particles, which can be corrected with increased data sampling at high angles. In addition, we recognize that non-linear charged particle dynamics is an active research area in machine learning, including at the Joint Institute of Nuclear Research [42] and the Large Hadron Collider [43, 44]. Machine learning predictions for electrospray particle dynamics will improve as a part of this growing nonlinear particle dynamics machine learning community.

The UCLA PESPL is actively pursuing multiple electrospray plume evolution research endeavors utilizing the DELI Model. The presented machine learning analysis compliments ongoing analytical research into plume divergence, drawing on beam characterization metrics from the particle accelerator community[45, 46]. Force analysis on DELI Model simulation data is also underway to determine a bounding spatial threshold beyond which simulated Coulomb interactions may be mathematically approximated without sacrificing accuracy in the resulting plume evolution. All research efforts share the objective of further illuminating the governing physics of electrospray plume evolution to inform thruster designs which optimize lifetime and performance.

Acknowledgments

The authors thank Adam Collins and Richard Obenchain for their insightful discussions of this work. This research was supported by the Air Force Office of Scientific Research (AFOSR) [Award No. FA9550-21-1-0067] and the NASA Jet Propulsion Laboratory (JPL) [Award No. 1580267].

References

- [1] Yamashita, M., and Fenn, J. B., "Electrospray ion source. Another variation on the free-jet theme," *The Journal of Physical Chemistry*, Vol. 88, No. 20, 1984, pp. 4451–4459. https://doi.org/10.1021/j150664a002, URL https://doi.org/10.1021/j150664a002.
- [2] Steipel, R. T., Gallovic, M. D., Batty, C. J., Bachelder, E. M., and Ainslie, K. M., "Electrospray for generation of drug delivery and vaccine particles applied *in vitro* and *in vivo*," *Materials Science & Engineering: C, Materials for biological applications*, Vol. 105, 2019, p. 1110070. https://doi.org/10.1016/j.msec.2019.110070.
- [3] Krupa, A., Jaworek, A., Sobczyk, A. T., Marchewicz, A., Szudyga, M., and Antes, T., "Charged spray generation for gas cleaning applications," *Journal of Electrostatics*, Vol. 71, No. 3, 2013, pp. 260–264. https://doi.org/https://doi.org/10.1016/j.elstat. 2012.11.022, URL https://www.sciencedirect.com/science/article/pii/S0304388612001362, journal of ELECTROSTATICS, Electrostatics 2013 12th International Conference on Electrostatics.

- [4] Cadnum, J. L., Jencson, A. L., Livingston, S. H., Li, D. F., Redmond, S. N., Pearlmutter, B., Wilson, B. M., and Donskey, C. J., "Evaluation of an electrostatic spray disinfectant technology for rapid decontamination of portable equipment and large open areas in the era of SARS-CoV-2," *American Journal of Infection Control*, 2020, pp. 951–954. https://doi.org/10.1016/j.ajic.2020.06.002.
- [5] Jaworek, A., Balachandran, W., Lackowski, M., Kulon, J., and Krupa, A., "Multi-nozzle electrospray system for gas cleaning processes," *Journal of Electrostatics*, Vol. 64, No. 3, 2006, pp. 194–202. https://doi.org/https://doi.org/10.1016/j.elstat.2005.05. 006, URL https://www.sciencedirect.com/science/article/pii/S0304388605001580.
- [6] Huang, C., Jian, G., Delisio, J. B., Wang, H., and Zachariah, M. R., "Electrospray Deposition of Energetic Polymer Nanocomposites with High Mass Particle Loadings: A Prelude to 3D Printing of Rocket Motors," *Advanced Engineering Materials*, Vol. 17, 2015.
- [7] Taylor, A. P., and Velásquez-García, L. F., "Electrospray-printed nanostructured graphene oxide gas sensors," *Nanotechnology*, Vol. 26, 2015, p. 505301. https://doi.org/10.1088/0957-4484/26/50/505301.
- [8] Ziemer, J., Marrese-Reading, C., Dunn, C., Romero-Wolf, A., Cutler, C., Javidnia, S., Le, T., Vi, I., Franklin, G., and Barela, P., "Colloid Microthruster Flight Performance Results from Space Technology 7 Disturbance Reduction System," *The 35th International Electric Propulsion Conference*, 2017, p. 20170010216.
- [9] Gaudi, B., Seager, S., Mennesson, B., Kiessling, A., Warfield, K., and Mawet, D., "The Habitable Exoplanet Observatory," Nature Astronomy, Vol. 2, 2018, pp. 600–604. https://doi.org/10.1038/s41550-018-0549-2.
- [10] Wang, F., Elbadawi, M., Tsilova, S. L., Gaisford, S., Basit, A. W., and Parhizkar, M., "Machine learning predicts electrospray particle size," *Materials & Design*, Vol. 219, 2022, p. 110735. https://doi.org/https://doi.org/10.1016/j.matdes.2022.110735, URL https://www.sciencedirect.com/science/article/pii/S0264127522003574.
- [11] Mayhew, A. W., Topping, D. O., and Hamilton, J. F., "New Approach Combining Molecular Fingerprints and Machine Learning to Estimate Relative Ionization Efficiency in Electrospray Ionization," *ACS Omega*, Vol. 5, No. 16, 2020, pp. 9510–9516. https://doi.org/10.1021/acsomega.0c00732, URL https://doi.org/10.1021/acsomega.0c00732, pMID: 32363303.
- [12] Gañán-Calvo, A., Lasheras, J., Dávila, J., and Barrero, A., "The electrostatic spray emitted from an electrified conical meniscus," *Journal of Aerosol Science*, Vol. 25, No. 6, 1994, pp. 1121–1142. https://doi.org/https://doi.org/10.1016/0021-8502(94)90205-4, URL https://www.sciencedirect.com/science/article/pii/0021850294902054.
- [13] Gastaño, M., "The structure of electrospray beams in vacuum," *Journal of Fluid Mechanics*, Vol. 604, 2008, p. 339–368. https://doi.org/10.1017/S0022112008001316.
- [14] Gamero-Castaño, M., and Galobardes-Esteban, M., "Electrospray propulsion: Modeling of the beams of droplets and ions of highly conducting propellants," *Journal of Applied Physics*, Vol. 131, No. 1, 2022, p. 013307. https://doi.org/10.1063/5.0073380, URL https://doi.org/10.1063/5.0073380.
- [15] Grifoll, J., and Rosell-Llompart, J., "Efficient Lagrangian simulation of electrospray droplets dynamics," *Journal of Aerosol Science*, Vol. 47, 2012, pp. 78–93. https://doi.org/https://doi.org/10.1016/j.jaerosci.2012.01.001, URL https://www.sciencedirect.com/science/article/pii/S0021850212000109.
- [16] Petro, E. M., Gallud, X., Hampl, S. K., Schroeder, M., Geiger, C., and Lozano, P. C., "Multiscale modeling of electrospray ion emission," *Journal of Applied Physics*, Vol. 131, No. 19, 2022, p. 193301. https://doi.org/10.1063/5.0065615, URL https://doi.org/10.1063/5.0065615.
- [17] Breddan, M. J., and Wirz, R. E., "Electrospray plume evolution: Influence of drag," *Journal of Aerosol Science*, Vol. 167, 2023, p. 106079. https://doi.org/10.1016/j.jaerosci.2022.106079, URL https://www.sciencedirect.com/science/article/pii/S002185022200115X.
- [18] F.R.S., L. R., "On the Stability, or Instability, of certain Fluid Motions," *Proceedings of the London Mathematical Society*, Vol. s1-11, No. 1, 1879, pp. 57–72. https://doi.org/https://doi.org/10.1112/plms/s1-11.1.57, URL https://londmathsoc.onlinelibrary. wiley.com/doi/abs/10.1112/plms/s1-11.1.57.
- [19] Mehta, N. A., and Levin, D. A., "Electrospray molecular dynamics simulations using an octree-based Coulomb interaction method," *Phys. Rev. E*, Vol. 99, 2019, p. 033302. https://doi.org/10.1103/PhysRevE.99.033302, URL https://link.aps.org/doi/10. 1103/PhysRevE.99.033302.
- [20] Gamero-Castaño, M., and de la Mora, J. F., "Electric-Field-Induced Ion Evaporation from Dielectric Liquids," *Physical Review Letters*, Vol. 89, 2002, p. 147602. https://doi.org/10.1103/PhysRevLett.89.147602.

- [21] Enomoto, T., Parmar, S. M., Yamada, R., Wirz, R. E., and Takao, Y., "Molecular Dynamics Simulations of Ion Extraction from Nanodroplets for Ionic Liquid Electrospray Thrusters," *Journal of Electric Propulsion*, Vol. 1, No. 1, 2022, p. 13. https://doi.org/10.1007/s44205-022-00010-1.
- [22] Yang, S., Wang, Z., Kong, Q., and Li, B., "Varicose-whipping instabilities transition of an electrified micro-jet in electrohydro-dynamic cone-jet regime," *International Journal of Multiphase Flow*, Vol. 146, 2022, p. 103851. https://doi.org/10.1016/j.ijmultiphaseflow.2021.103851, URL https://www.sciencedirect.com/science/article/pii/S0301932221002731.
- [23] Collins, A. L., Uchizono, N. M., Huh, H., and Wirz, R. E., "Three-Dimensional Microscopy and Analysis of the Emission Cone Meniscus for Electrospray Thrusters," *37th International Electric Propulsion Conference*, 2022, pp. IEPC–2022–228.
- [24] Uchizono, N. M., Collins, A. L., Thuppul, A., Wright, P. L., Eckhardt, D. Q., Ziemer, J., and Wirz, R. E., "Emission Modes in Electrospray Thrusters Operating with High Conductivity Ionic Liquids," *Aerospace*, Vol. 7, No. 10, 2020. https://doi.org/10.3390/aerospace7100141, URL https://www.mdpi.com/2226-4310/7/10/141.
- [25] Grifoll, J., A., A. K., and Rosell-Llompart, J., "Numerical Simulation of Electrospray Droplets Dynamics," *V Reunion Esponola de Ciecia y Tecnologia de Aerosoles (RECTA)*, 2011.
- [26] Breddan, M. J., and Wirz, R. E., "Machine Learning Electrospray Plume Dynamics,", 2023. Accepted for publication to Engineering Applications of Artificial Intelligence in 2023.
- [27] Pedregosa, F., Varoquaux, G., Gramfort, A., Michel, V., Thirion, B., Grisel, O., Blondel, M., Prettenhofer, P., Weiss, R., Dubourg, V., Vanderplas, J., Passos, A., Cournapeau, D., Brucher, M., Perrot, M., and Édouard Duchesnay, "Scikit-Learn: Machine Learning in Python," *Journal of Machine Learning Research*, Vol. 12, No. null, 2011, p. 2825–2830.
- [28] Chen, T., and Guestrin, C., "XGBoost: A Scalable Tree Boosting System," Proceedings of the 22nd ACM SIGKDD International Conference on Knowledge Discovery and Data Mining, Association for Computing Machinery, New York, NY, USA, 2016, p. 785–794. https://doi.org/10.1145/2939672.2939785, URL https://doi.org/10.1145/2939672.2939785.
- [29] Ke, G., Meng, Q., Finley, T., Wang, T., Chen, W., Ma, W., Ye, Q., and Liu, T.-Y., "LightGBM: A Highly Efficient Gradient Boosting Decision Tree," *Advances in Neural Information Processing Systems*, Vol. 30, edited by I. Guyon, U. V. Luxburg, S. Bengio, H. Wallach, R. Fergus, S. Vishwanathan, and R. Garnett, Curran Associates, Inc., 2017. URL https://proceedings.neurips.cc/paper/2017/file/6449f44a102fde848669bdd9eb6b76fa-Paper.pdf.
- [30] Breddan, M. J. D., Curry, D. R., Sharma, M. R., Richmond, M. O., Collins, A. L., and Wirz, R. E., "Electrospray Plume Modeling: Study on Drag Influence," AIAA Science and Technology Forum and Exposition, 2022, pp. AIAA–2022–1358.
- [31] Rosell-Llompart, J., Grifoll, J., and Loscertales, I. G., "Electrosprays in the cone-jet mode: From Taylor cone formation to spray development," *Journal of Aerosol Science*, Vol. 125, 2018, pp. 2–31. https://doi.org/https://doi.org/10.1016/j.jaerosci. 2018.04.008, URL https://www.sciencedirect.com/science/article/pii/S0021850217304366, from Electro-Hydro-Dynamics of liquids for the production of charged droplets by Electro-Spray to applications for tailored Materials (aerosols, powders, coatings) and Environment.
- [32] Arumugham-Achari, A. K., Grifoll, J., and Rosell-Llompart, J., "A Comprehensive Framework for the Numerical Simulation of Evaporating Electrosprays," *Aerosol Science and Technology*, Vol. 49, No. 6, 2015, pp. 436–448. https://doi.org/10.1080/ 02786826.2015.1039639, URL https://doi.org/10.1080/02786826.2015.1039639.
- [33] Thuppul, A., Wright, P. L., Collins, A. L., Ziemer, J. K., and Wirz, R. E., "Lifetime Considerations for Electrospray Thrusters," Aerospace, Vol. 7, No. 8, 2020. https://doi.org/10.3390/aerospace7080108, URL https://www.mdpi.com/2226-4310/7/8/108.
- [34] Collins, A. L., Wright, P. L., Uchizono, N. M., and Wirz, R. E., "High angle mass flux of an electrospray plume," *Journal of Electric Propulsion*, Vol. 1, No. 1, 2022, p. 32. https://doi.org/10.1007/s44205-022-00031-w, URL https://doi.org/10.1007/s44205-022-00031-w.
- [35] Davis, M. J., Collins, A. L., and Wirz, R. E., "Electrospray Plume Evolution Via Discrete Simulation," *The 36th International Electric Propulsion Conference*, 2019, pp. IEPC–2019–590.
- [36] Thuppul, A., Collins, A. L., Wright, P. L., Uchizono, N. M., and Wirz, R. E., "Mass flux and current density distributions of electrospray plumes," *Journal of Applied Physics*, Vol. 130, No. 10, 2021, p. 103301. https://doi.org/10.1063/5.0056761, URL https://doi.org/10.1063/5.0056761.
- [37] Demmons, N., Hruby, V., Spence, D., Roy, T., Ehrbar, E., Zwahlen, J., Martin, R., Ziemer, J., and Randolph, T., "ST7-DRS mission colloid thruster development," 44th AIAA/ASME/SAE/ASEE Joint Propulsion Conference & Exhibit, 2008, p. 4823.

- [38] Wilhelm, O., M\u00e4dler, L., and Pratsinis, S., "Electrospray evaporation and deposition," *Journal of Aerosol Science*, Vol. 34, No. 7, 2003, pp. 815–836. https://doi.org/https://doi.org/10.1016/S0021-8502(03)00034-X, URL https://www.sciencedirect.com/science/article/pii/S002185020300034X.
- [39] Arumugham Achari, A. K., Grifoll, J., and Rosell-Llompart, J., "Numerical simulations of evaporating electrosprays with Coulomb explosions," *Aerosol Technologies*, 2014.
- [40] Magnusson, J. M., Collins, A. L., and Wirz, R. E., "Polyatomic Ion-Induced Electron Emission (IIEE) in Electrospray Thrusters," Aerospace, Vol. 7, No. 11, 2020. https://doi.org/10.3390/aerospace7110153, URL https://www.mdpi.com/2226-4310/7/11/153.
- [41] Uchizono, N. M., Collins, A. L., Marrese-Reading, C., Arestie, S. M., Ziemer, J. K., and Wirz, R. E., "The role of secondary species emission in vacuum facility effects for electrospray thrusters," *Journal of Applied Physics*, Vol. 130, No. 14, 2021, p. 143301. https://doi.org/10.1063/5.0063476, URL https://doi.org/10.1063/5.0063476.
- [42] Roudnev, V. A., Merts, S. P., Nemnyugin, S. A., and Stepanova, M. M., "Machine learning based TOF charged particle identification at BM@N detector of NICA collider," *Journal of Physics: Conference Series*, Vol. 1479, 2020, p. 012043. https://doi.org/10.1088/1742-6596/1479/1/012043, URL https://iopscience.iop.org/article/10.1088/1742-6596/1479/1/012043.
- [43] Abidi, H., Boveia, A., Cavaliere, V., Furletov, D., Gekow, A., Kalderon, C. W., and Yoo, S., "Charged Particle Tracking with Machine Learning on FPGAs,", 2022.
- [44] Våge, L. H., "Reinforcement learning for charged-particle tracking," *Connecting the Dots Workshop (CTD)*, 2022, pp. PROC–CTD2022–37.
- [45] Sorensen, A. H., "INTRODUCTION TO INTRABEAM SCATTERING," Conf. Proc. C, Vol. 860915, 1986, pp. 135 152.
- [46] Sørensen, A., "Liouville's theorem and emittance," 1989. https://doi.org/10.5170/CERN-1989-005.18, URL https://cds.cern. ch/record/367259.